Metaconcrete: designed aggregates to enhance dynamic performance

Stephanie J. Mitchell [a], Anna Pandolfi [b,*], Michael Ortiz [a]

[a] EAS Division, California Institute of Technology, Pasadena, CA 91125, USA
[b] DICA, Politecnico di Milano, 20133 Milano, Italy

Article history:
Received 18 June 2013
Received in revised form
5 October 2013
Accepted 13 January 2014
Available online 1 February 2014

1. Introduction

Recently, a significant progress has been made in the design of new materials engineered to have unconventional properties. Termed metamaterials, these complex composites gain their properties not from the chemical composition of their components, but instead from the rigorously designed microstructure. Metamaterials can be designed to display unusual material behavior when subject to electromagnetic, acoustic, or elastic waves. They may exhibit properties such as negative refractive index, negative bulk modulus, or negative mass; properties which are desirable for many engineering purposes but not typically observable in materials found in nature. The unique properties of metamaterials are often gained through the use of inclusions and structural features that are significantly smaller than the wavelength of waves with which they interact.

Earlier studies on metamaterials investigated the possibility of materials with negative refractive index at optical wavelengths. Pendry (2000) proposed the idea of superlenses with spatial resolution below that of the wavelength of light.

* Corresponding author.
E-mail address: anna.pandolfi@polimi.it (A. Pandolfi).

Kundtz and Smith (2010) demonstrated a form of invisibility over a narrow wave band with gradient-index materials. The development of metamaterials for the manipulation of electromagnetic waves has also led to the consideration of acoustic and seismic metamaterials, which are currently areas of active research.

There has been considerable attention placed on the development of sonic or phononic crystals for use in acoustic metamaterials (Kushwaha et al., 1993; Klironomos and Economou, 1998; Psarobas et al., 2000; Goffaux and Sánchez-Dehesa, 2003; Jensen, 2003; Hirsekorn, 2004; Wang et al., 2004a; Wang et al., 2004a–c). Analogous to the photonic crystals used in the attenuation of electromagnetic waves, these periodic composite materials exhibit wave filtering behavior, creating band gaps or stop bands within the frequency spectrum. Within the band gap frequency range, the applied acoustic or elastic waves cannot propagate and the incident energy is dispersed or scattered from the medium. These metamaterials often make use of Bragg-type band gaps (Goffaux and Sánchez-Dehesa, 2003; Hirsekorn, 2004; Wang et al., 2004c), where the periodicity of the structure induces vibration reduction within the material. However, inducing Bragg gaps in the low frequency range requires the internal structure to have a spatial period of similar size to the wavelength of the incoming wave. The wavelength of low frequency elastic waves in typical solids is relatively long in comparison to the dimensions of a typical acoustic shelter, thus making the use of Bragg gaps alone impractical for insulating acoustic waves.

To overcome this problem, Liu et al. (2000) developed an array of locally resonant inclusions, consisting of silicone coated lead spheres in an epoxy matrix. When a sonic wave passes through the material, resonance of the internal lead sphere can be activated at chosen frequencies, creating resonance induced band gaps two orders of magnitude lower than that obtained by the Bragg limit. Liu et al. (2002) demonstrated that the configuration of the band-gap can be tuned continuously from a resonance gap to a Bragg gap by varying the elastic properties of the inclusion components. A softer coating led to a resonance gap, whereas a stiff coating material created an elastic wave gap derived from Bragg scattering.

The wave attenuation behavior of acoustic metamaterials is derived from the unusual material properties that these composites display, such as negative effective mass or negative bulk modulus. Liu et al. (2000) demonstrated that disordered composites constructed with locally resonant inclusions display negative effective material properties, breaking the conventional mass–density law of sound transmission. Mass density is typically considered to be the volume average of the constituents. However, in the case of resonant inclusions there is relative motion between the constituents and the matrix (Mei et al., 2006). This induces a change in the mass density of the composite, meaning that the effective mass density for the dynamic case is different from that in the static configuration. The effective mass density can also become negative in value when the core of the inclusion resonates, leading to interesting and unusual interactions with the applied wave motion. The concept of effective mass density has also been studied by Sheng et al. (2003, 2007) and Liu et al. (2002, 2005, 2011).

To further investigate the design of locally resonant metamaterials, Wang et al. (2006) studied longitudinal wave propagation in a quasi-one-dimensional slender beam with periodically attached harmonic oscillators. They computed the transmission frequency response function for the system and performed vibration experiments on a laboratory setup with an arrangement of masses and springs resembling the theoretical model, observing good correspondence between the two results. Wang et al. also found analytically that the beam to inclusion coating stiffness ratio highly influenced the attenuation properties within the observed transmission frequency band gap. Xiao et al. (2012) extended this work, modeling a uniform elastic rod containing a periodic array of multi-degree-of-freedom resonators, developing a methodology to predict the complex band structure resulting from these metamaterials. The inclusion of multi-degree-of-freedom resonators resulted in the presence of multiple band gaps, often achieving greater attenuation performance than in the single-degree-of-freedom case. Through a parametric study, they were able to show that there exists coupling between both the Bragg-type and resonance-type gaps present in the response. This coupling behavior resulted in a great improvement in the bandwidth and attenuation performance of gaps around Bragg conditions, leading to super-wide band gaps useful in broadband vibration control applications.

There have been a number of recent efforts in the development of analytic modeling tools for metamaterials containing inclusions and other complex microstructures. Milton and Willis (2007) presented a rigorous framework involving what they term the Willis equations, introducing a new point of view on the elastodynamic equations of composite materials. They consider the harmonic motion of a rigid body with hidden spring–mass systems, using a number of configurations to explain the concept of negative effective mass density in simple metamaterials with resonators. Using Newton's law for the motion of the included mass, they derive generalized equations of motion for the rigid body, where the effective mass (or p-mass) is a function of the oscillation frequency. Near the resonance frequency of the spring–mass system the p-mass assumes large values, becoming complex and eventually negative.

Zhu et al. (2011) used the same metamaterial proposed by Milton and Willis (2007) to develop a microstructure continuum model as an alternative to classic continuum theory. They derived field equations to represent elastic metamaterials with resonator microstructures, and used these in comparison with the finite element method to show accurate prediction of band gap features. Liu et al. (2012) took a similar approach, developing a multi-displacement microstructure continuum model to obtain the macroscopic governing equations for an anisotropic elastic metamaterial consisting of an epoxy matrix with lead cylinders coated with an elliptically shaped soft layer. Milton et al. (2006) and Milton (2007) also discussed metamaterials in the context of elastic cloaking devices, developing theory that may be useful for design of composites that can cloak objects from elastic waves of a given frequency. It is also possible to utilize an optimization approach to the development of engineered materials with unusual properties. Sigmund and Torquato (1997), Sigmund (2000) and Gibiansky and Sigmund (2000) used topology optimization to generate ideal materials which exhibit

properties such as vanishing thermal expansion or negative Poisson's ratio. These techniques provide a way of designing optimal microstructures for composites such as metamaterials.

In the present study, we investigate from both the theoretical and numerical point of view a new concept for concrete in structural applications. Specifically, in our concrete, standard aggregates are replaced by bi-material inclusions that modify the dynamic response of the system over the frequency spectra typical of fast dynamical actions. These new aggregates are spherical inclusions consisting of a heavy metal core (e.g. lead) coated with a layer of soft material, possibly encapsulated inside a thin steel protective case. Under the action of particular frequencies, the aggregates show a resonant behavior by oscillating about their equilibrium configuration and consequently trapping a portion of the supplied mechanical energy of the system. We name this particular composite *metaconcrete*. Resonant aggregates characterize metaconcrete with a wide range of high natural frequencies not observed in regular concrete. Standard concrete aggregates consist of stone, gravel, and sand whose density and stiffness are similar to those of the mortar matrix; thus, although standard concrete is a true composite, for most applications where the elastic behavior is dominant, it can be considered to be a homogeneous material. Conversely, metaconcrete is non-homogeneous because of the particular choice of aggregates.

We consider uniformly sized metaconcrete aggregates. We show that the volumetric proportion of the metaconcrete components and their corresponding mechanical properties can be tuned in order to adjust the range of natural frequencies covered by the system. Using resonant aggregates of different sizes may provide additional functionality to the material, by enabling a larger range of natural frequencies. We will show that the mechanical behavior of metaconcrete differs from that of regular concrete. Resonant aggregates are able to trap a portion of the supplied energy and to activate localized oscillatory motions characterized by an exchange of elastic energy and kinetic energy between the stiff core and the soft outer coating. The global effect is to reduce the stress in the mortar phase, enhancing its ability to sustain the applied dynamical actions without damage.

Particularly interesting applications of metaconcrete are explosive blast shielding structures, protective slabs against impacts, and tuned damping foundations to mitigate seismic actions in buildings, see also Brun et al. (2009).

The paper is structured as follows. In Section 2, after recalling the concept of effective momentum mass introduced in Milton and Willis (2007), we provide an estimate of the natural frequency of a metaconcrete aggregate and identify the geometrical and material parameters that affect resonance behavior. We present finite element models of metaconcrete slabs in Section 3, and examine numerically their behavior under the action of a blast due to the ignition of an explosive. In Section 4 we provide some design indications for the soft coating in order to define a metaconcrete able to reduce the transmitted mechanical energy and the maximum stress in the mortar phase. Concluding remarks are given in Section 5, and we outline a plan for future experimental testing of metaconcrete prototypes and the integration of numerical studies with the inclusion of brittle and rate-dependent behaviors.

2. Tuning the metaconcrete aggregates

The metaconcrete aggregates must be tuned so that resonant oscillations of the internal mass are induced as the blast wave propagates through the material. Resonance within the inclusions is linked to the concept of negative effective mass, which creates the favorable wave attenuation properties of metaconcrete. In order to engineer the aggregates to perform as devised, we must also investigate how the material properties of each phase in the aggregate influence the resonant behavior.

2.1. Negative mass concept

We introduce the concept of negative mass by briefly recalling the elementary example described in Milton and Willis (2007). Milton and Willis considered a one-dimensional model consisting of n cylindrical cavities of length d, carved out from a bar of rigid material with mass m_0. In each cavity, a mass m is connected to the walls through two springs of stiffness k, as illustrated in Fig. 1. The system oscillates harmonically in time with frequency ω under the action of the external force $f(t)$. The spring forces acting on the right and left side of each mass are denoted $f_r(t)$ and $f_l(t)$, respectively. All the forces vary in time according to

$$f(t) = \mathrm{Re}(Fe^{-i\omega t}),$$
$$f_r(t) = \mathrm{Re}(F_r e^{-i\omega t}),$$
$$f_l(t) = \mathrm{Re}(F_l e^{-i\omega t}),$$

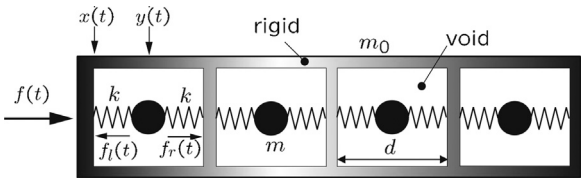

Fig. 1. A one-dimensional material where the 'effective' mass depends on the frequency ω and can be negative (Milton and Willis, 2007).

where capital symbols denote complex numbers. The position of the left wall and of the first mass are denoted by the coordinates $x(t)$ and $y(t)$ respectively, with

$$x(t) = \mathrm{Re}\left(U_x e^{-i\omega t}\right), \quad y(t) = \frac{d}{2} + \mathrm{Re}\left(U_y e^{-i\omega t}\right),$$

where U_x and U_y are the complex displacements of the rigid system and of the mass, respectively. The velocities follow as

$$v_x(t) = \mathrm{Re}(V_x e^{-i\omega t}), \quad v_y(t) = \mathrm{Re}(V_y e^{-i\omega t}),$$

with

$$V_x = -i\omega U_x, \quad V_y = -i\omega U_y$$

and accelerations are

$$a_x(t) = \mathrm{Re}(A_x e^{-i\omega t}), \quad a_y(t) = \mathrm{Re}(A_y e^{-i\omega t}),$$

with

$$A_x = -i\omega V_x = \omega^2 U_x, \quad A_y = -i\omega V_y = \omega^2 U_y. \tag{1}$$

The equation of motion of the rigid body is

$$F - n(F_l - F_r) = m_0 A_x \tag{2}$$

and the equation of motion for each mass m is

$$F_l - F_r = mA_y. \tag{3}$$

The forces of the springs can be expressed in terms of the displacement by using Hooke's law

$$F_l - F_r = 2k(U_y - U_x), \tag{4}$$

leading to

$$2k(U_y - U_x) = 2k\frac{A_y - A_x}{\omega^2} = mA_y, \tag{5}$$

from where the expression of A_y can be derived

$$A_y = \frac{2k}{2k - m\omega^2} A_x. \tag{6}$$

By combining (2), (3) and (6) we obtain

$$F = M(\omega)A_x, \quad M(\omega) = m_0 + \frac{2knm}{2k - m\omega^2}.$$

The mass M is called the effective momentum mass or p-mass. The p-mass reduces to the rigid body mass m_0 for vanishing spring stiffness, and to the sum of the masses $m_0 + nm$ in the absence of motion. If we introduce the natural frequency of one of the mass–spring cores as

$$\omega_\rho = \sqrt{\frac{2k}{m}} \tag{7}$$

we can write the p-mass as

$$M(\omega) = m_0 \left(1 + \alpha \frac{\omega_\rho^2}{\omega_\rho^2 - \omega^2}\right), \quad \alpha = \frac{nm}{m_0}. \tag{8}$$

The p-mass can become huge and complex near resonances and achieve negative values for $\omega > \omega_\rho$, as seen in Fig. 2.

2.2. Resonant aggregates

With the help of a mass–spring system equivalent to the resonant aggregate, we derive a simple relationship that combines the main geometry parameters along with the stiffness of the soft coating. This relation can be used to define the range of resonant frequencies for an ideal metaconcrete. Let us consider a single inclusion, where we choose a heavy core consisting of lead with a radius R_l and a soft material coating of thickness t. The density of lead is denoted ρ_l, and the total mass of the heavy core is

$$m = \rho_l \frac{4}{3}\pi R_l^3. \tag{9}$$

The stiffness of the surrounding soft material can be assumed, on each side, to be equivalent to a spring of constant k

$$k = \frac{E_s A}{t}, \tag{10}$$

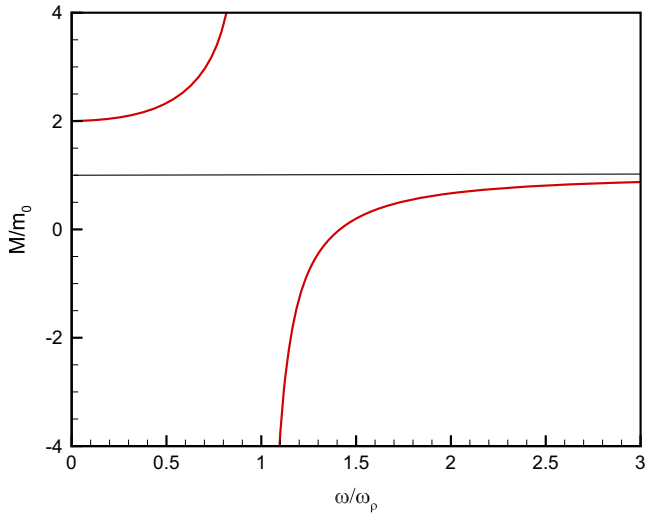

Fig. 2. Variation of the p-mass value with the excitation frequency of the model described in Milton and Willis (2007).

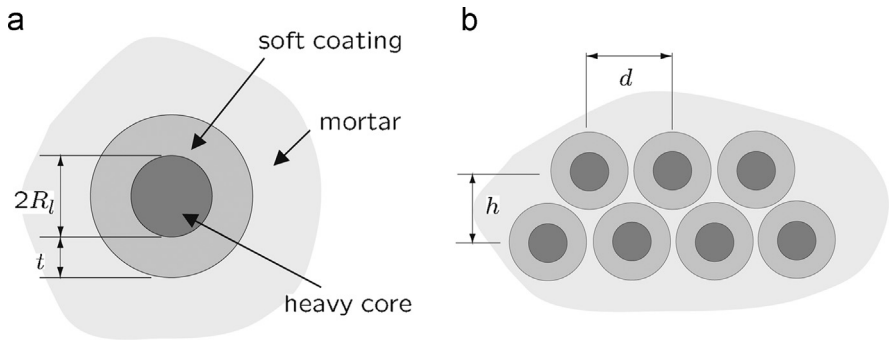

Fig. 3. (a) Geometry and structure of the aggregates, consisting of a heavy core of radius R_l and a soft coating of thickness t. (b) Geometrical assembly of the aggregates in a regular two-dimensional arrangement, characterized by heavy cores located at central distances of magnitude d and h.

where $A=\pi R_l^2$ is proportional to the lead core maximum section area, i.e., the portion of soft material resisting the motion of the core. The resonant frequency of a one-dimensional system of mass m and with two equivalent springs of stiffness k is therefore given by

$$\omega^2=\frac{2k}{m} \tag{11}$$

and combining Eqs. (9)–(11):

$$\omega^2=\frac{3}{2}\frac{E_s}{R_l t\rho_l}. \tag{12}$$

For an assigned frequency $\omega=\overline{\omega}$, Eq. (12) provides the optimal combination of geometry and mechanical properties of the aggregates. In particular, for an assigned geometry one can estimate the appropriate material stiffness E_s as

$$E_s=\frac{2}{3}R_l t\rho_l\overline{\omega}^2. \tag{13}$$

Likewise, for an assigned material, the geometrical term $R_l t$ is given by

$$R_l t=\frac{3}{2}\frac{E_s}{\rho_l\overline{\omega}^2}, \tag{14}$$

which provides an approximate definition of the aggregate size. The variation of the elastic modulus E_s and the aggregate size $R_l t$ with the resonant frequency are visualized in Fig. 4(a) and (b), respectively. The figures provide interesting design suggestions according to the function desired of the metaconcrete. For the material to be employed as protection against blast loading, the metaconcrete must behave as a resonant material at high frequencies, since blast pressure histories are characterized by high frequency spectra. Adopting a stiff coating material and a small aggregate size achieves the high

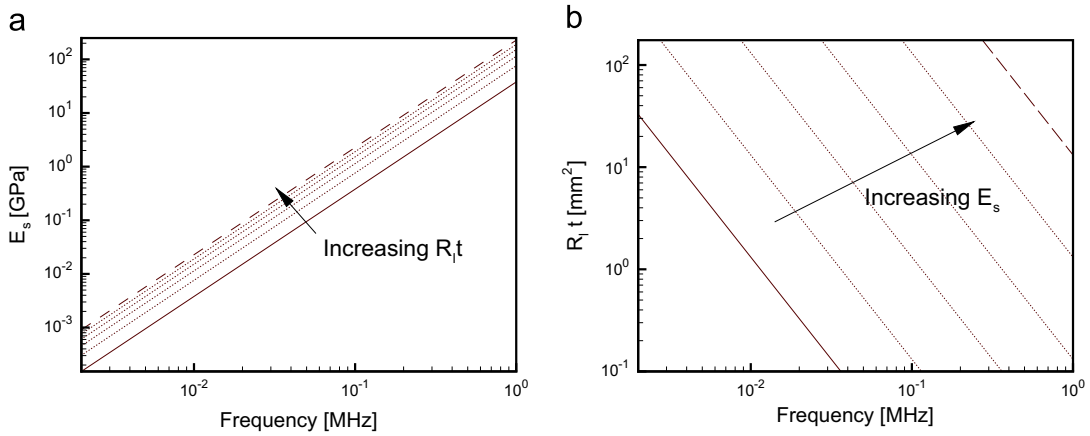

Fig. 4. Dependence of aggregate parameters on the resonant frequency. (a) Elastic modulus of the soft coating. Lines correspond to different aggregate sizes $R_l t$, from 5 mm^2 (solid line) to 30 mm^2 (broken line). (b) Size of the aggregate. Lines correspond to different elastic moduli E_s, from 0.001 GPa (solid line) to 100 GPa (broken line).

Table 1
Material constants used in the simulations.

Material	ρ (kg/m^3)	E_s (GPa)	ν
Mortar	2500	30	0.20
Lead	11,400	16	0.44
Silicone	1100	0.001	0.47
Natural rubber	900	0.01	0.49
Low density polyethylene	1100	0.1	0.45
Nylon	1150	1.0	0.40
Urea formaldehyde	1500	10	0.40

resonant frequencies desired, as seen in Fig. 4(a). For the case of protection against earthquakes, whose frequencies are in the range 0.01–10 Hz, the aggregates must be of larger size and a lower value of elastic modulus must be chosen, see Fig. 4(b).

Possible coating materials covering an elastic modulus range of 1 MPa to 10 GPa are listed in Table 1. Also listed are the properties of the mortar matrix, along with those of the core material, chosen to be lead for the purposes of this numerical investigation.

3. Finite element models

To further characterize the behavior of metaconcrete under the action of blast loading, we employ a model of simple geometry that will enable the dynamical effects to be easily understood. We consider an infinite planar slab of thickness L and restrict our attention to a square cross section of material spanning the entire slab thickness, see Fig. 5. The concrete portion is constrained not to deform in the slab plane. The size b of the sample is chosen to be significantly smaller than the slab thickness and close to the actual size of the aggregates, which are arranged in a regular way at a distance d one from another, see Fig. 3(b). Geometrical constraints impose the restriction:

$$2(R_l + t) \le d. \tag{15}$$

To increase the density of the aggregates, we model quarters of aggregate along the longitudinal edges, at a distance $h = d\sqrt{3}/2$ from the center of the aligned aggregates, see Fig. 3(b). The total volume and the total weight of the system can be expressed in terms of the components of volume and weight, or

$$V_{\text{tot}} = V_m + V_s + V_l, \quad W_{\text{tot}} = V_m\rho_m + V_s\rho_s + V_l\rho_l, \tag{16}$$

where V_i and ρ_i denote, respectively, the volume and the density of the component i. Indices m, s and l refer to the mortar, soft coating and lead phases, respectively. The volume fractions of the components v_i and the filling fraction of the aggregates in terms of weight f_a are defined as follows:

$$v_i = \frac{V_i}{V_{\text{tot}}}, \quad f_a = \frac{1}{W_{\text{tot}}}\left(V_s\rho_s + V_l\rho_l\right). \tag{17}$$

In the present study, we assume $L = 0.24$ m, $b = 0.03$ m, and $R_l + t = 12$ mm, and we vary R_l and t according to the values reported in Table 2. The table lists the number of nodes and elements of the discretized solid, the volume ratios, and the

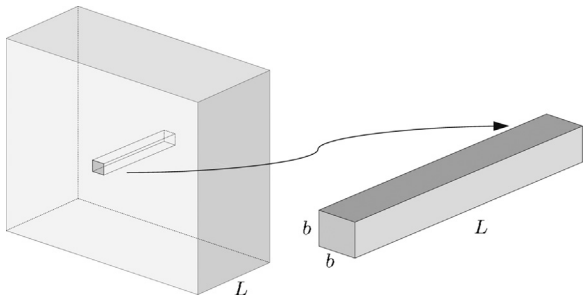

Fig. 5. Geometry of the concrete slab of thickness L, and the restricted slab portion of edge length b.

Table 2
Geometrical and discretization data.

Configuration	R_l (mm)	t (mm)	$R_l t$ (mm^2)	$\omega/2\pi$ (kHz)	V_m (%)	V_s (%)	V_l (%)	f_a (%)	Nodes	Elements
A	11	1	11	17.4	49.7	11.6	38.7	78.4–78.7	19,228	96,314
B	10	2	20	12.9	49.7	21.2	29.1	73.8–74.5	19,645	95,390
C	9	3	27	11.1	49.7	29.1	21.2	68.3–69.7	20,891	107,562

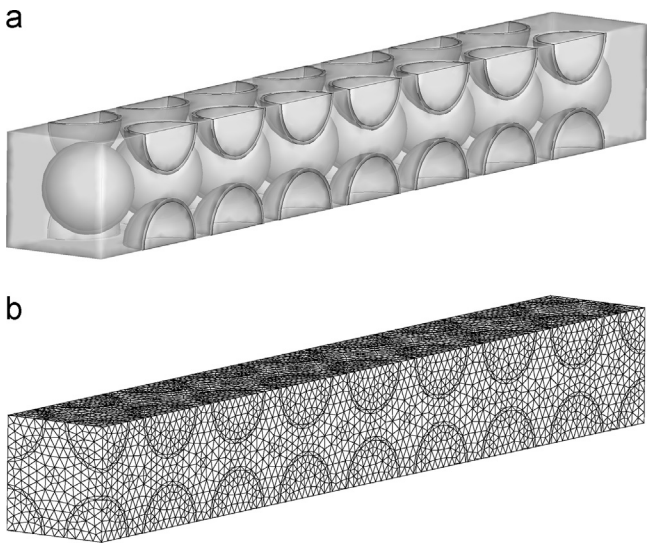

Fig. 6. Solid model and finite element discretization (mesh size $h=2.5$ mm) of the portion of slab. (a) Solid model and (b) finite element mesh.

filling ratios. The filling ratio varies according to the choice of the soft coating material. Table 2 also lists the resonant frequencies for each aggregate geometry, using the relation derived in Eq. (12) and a nylon inclusion coating.

Configuration A is visualized in Fig. 6(a). The solid model has been discretized with a uniform mesh size of 2.5 mm, which reduces, if necessary, to a smaller value within the soft layer according to the coating thickness, see Fig. 6(b). For all components, the material behavior is described by a neo-Hookean material model, extended to the compressible range, and adopting the material properties listed in Table 1.

The system is excited by a blast pressure history, which activates a large spectrum of frequencies. We assume that the blast is applied to the forward side of the slab, while the opposite side is free to move, and we apply periodic boundary conditions to the lateral surfaces. We assume a blast pressure history due to the ignition of a 10 kg TNT charge, located 0.015 m from the central point of the exposed surface. The model of the blast pressure used in the calculations is summarized in the Appendix; an accurate description of the blast in air can be found, e.g., in Kinney (1962). The blast force is characterized by the time history and the frequency spectrum. The total blast force at time t is given by the resultant of the blast pressures acting normally to the exposed surface A_{exposed}, i.e.

$$F(t) = \int_{A_{\text{exposed}}} p(t)\, dA. \tag{18}$$

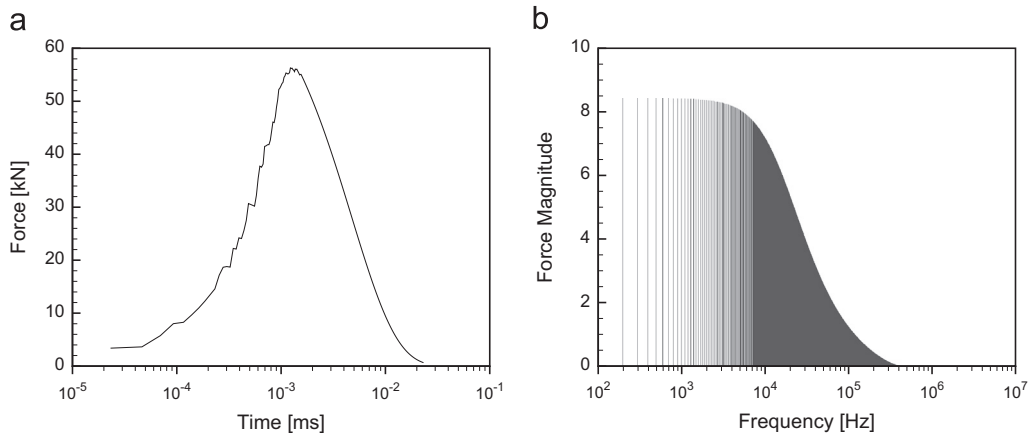

Fig. 7. (a) Variation in time of the resultant blast pressure on the exposed surface of the slab and (b) Fourier transform (signal magnitude) of the blast force.

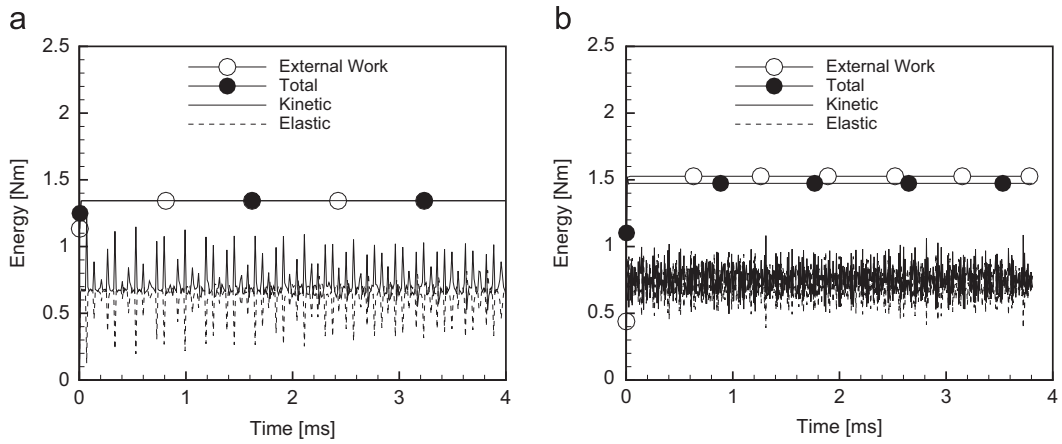

Fig. 8. Global system energy history: supplied energy (white circles), elastic energy (broken line), kinetic energy (solid line) and total mechanical energy of the system (black circles). (a) Standard concrete and (b) metaconcrete.

Fig. 7(a) shows the time history of the blast force. The frequency spectrum is obtained in terms of magnitude through the Fourier transform, see Fig. 7(b). For the present simulations, the blast pressure acts for a short time interval of less than 0.01 ms, and most of the excited frequencies are in the range between 1 kHz and 1 MHz.

We begin by providing a qualitative illustration of the behavior of metaconcrete when subject to a blast excitation. As an illustrative example, we first consider a metaconcrete slab consisting of nylon coated inclusions of the configuration denoted A in Table 2. We analyze this alongside a homogeneous slab with the effective properties of concrete, which provides us with a baseline for comparison. We evaluate the two materials using the energy history, which is shown in Fig. 8(a) for the case of the homogeneous material, and Fig. 8(b) for the chosen metaconcrete. In these figures, solid lines denote the total kinetic energy, broken lines the total elastic energy, black circles the total mechanical energy, and white circles the energy supplied to the system. The supplied energy is given by the external work done by the pressure forces on the impacted surface, or

$$W^{\text{ext}} = \int_0^t \int_{A_{\text{exposed}}} p(t)\, dA\, du(t), \tag{19}$$

where $du(t)$ is the incremental displacement component normal to the exposed area. Note that the amount of supplied energy differs depending on the configuration chosen for the metaconcrete and according to the choice of soft coating material. Since the applied force is equal, the difference is due to the magnitude of the displacement at the exposed surface. Fig. 8 shows clearly that the system is conservative; the supplied energy provides the total mechanical energy and a continuous exchange between kinetic energy and elastic energy is observed during the process.

Details concerning the partition of the energy between the three components of the metaconcrete system can be observed in Fig. 9. The plots show the time histories of the mechanical, kinetic, and elastic energy, for each component of the system. Solid lines denote the energy carried by the mortar, broken lines the energy carried by the soft coating, and dotted

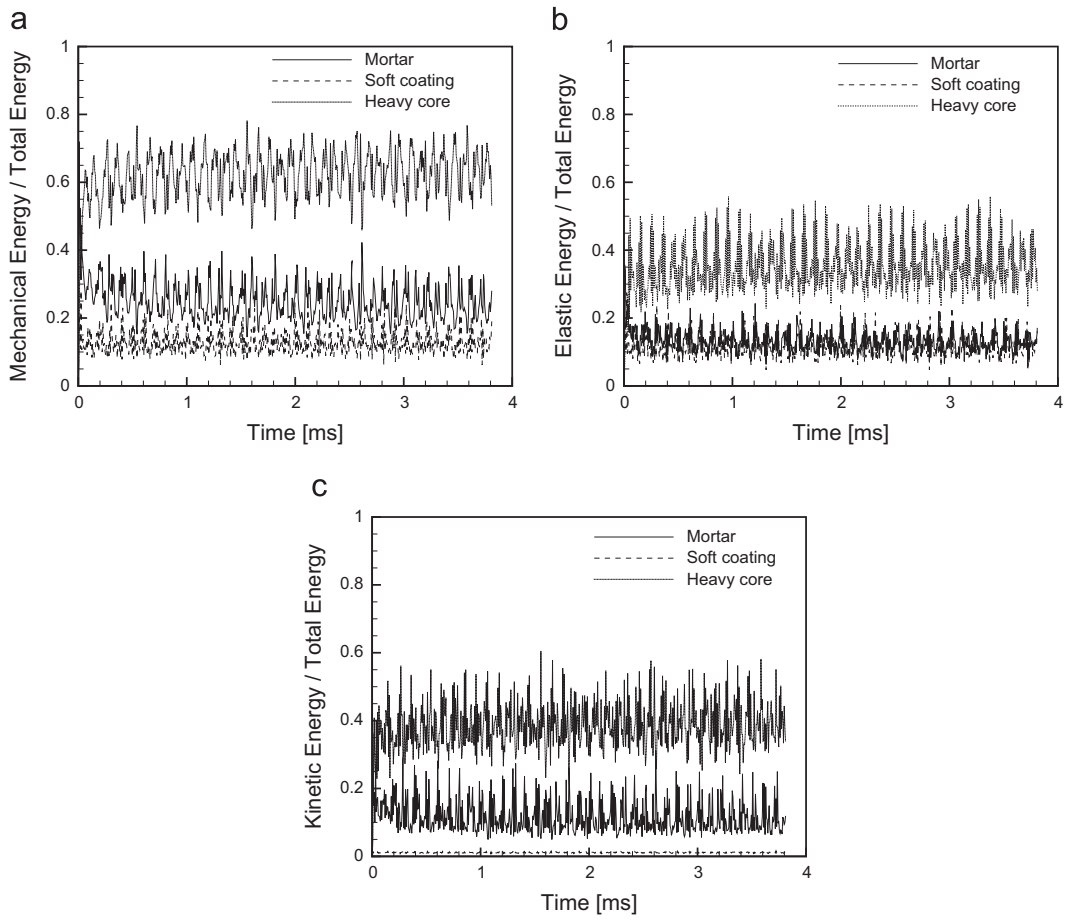

Fig. 9. Fractions of mechanical, elastic and kinetic energies carried by the three components of the metaconcrete, expressed with respect to the total mechanical energy of the system. (a) Mechanical energy, (b) elastic energy and (c) kinetic energy.

lines the energy carried by the lead cores. The energies are expressed with respect to the total mechanical energy of the system. For the configuration of metaconcrete considered, Fig. 9(a) shows that approximately 60% of the mechanical energy is carried by the lead cores, while the mortar carries 30%. Fig. 9(b) shows that the elastic energy in the mortar and in the soft coating is only one-third of the elastic energy in the lead cores, which undergo elastic oscillations. Fig. 9(c) shows that a large amount of kinetic energy remains trapped in the lead cores. Comparison of the plots suggests the presence of oscillatory motion of the lead cores inside the aggregates.

Further insight into this oscillatory behavior can be revealed by studying the longitudinal stress distribution along the surface of the mid-longitudinal cross-section of the slab. Fig. 10 compares the stress distribution a few tenths of a millisecond after the beginning of the blast in both the homogeneous material and the metaconcrete, where the blast surface is located at the left end of the section. At this point in the time history the compressive shock wave is traveling for the first time towards the back side of the slab. In the figure, dark gray shades denote compression and the lighter white shades denote tension. In the homogeneous material, the first shock wave travels at the velocity of the longitudinal wave speed while preserving a regular one-dimensional structure. In the metaconcrete slab the front shock wave propagates at lower speed, and the average magnitude of the longitudinal stress reduces with the distance from the blasted surface. The aggregates in turn are subject to elastic oscillations, which can be observed in the left side of Fig. 10(b). The resonant behavior can be seen in the second inclusion from the left; the lead core is under compression in the center and under tension in the annular region adjacent to the coating.

The features observed in this reference case characterize the behavior of all the considered configurations.

4. Influence of the soft phase elastic modulus and thickness

We perform a parametric study of the mechanical behavior of metaconcrete by varying the material properties (e.g., elastic modulus and density) and thickness of the soft coating. The results of the analyses are presented in terms of the

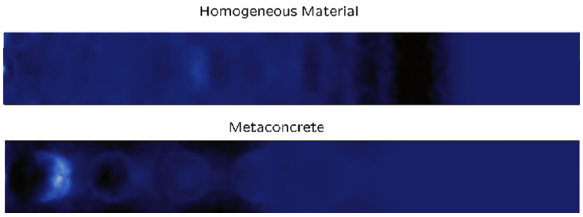

Fig. 10. Comparison of the distribution of longitudinal stress at the same time step between both a homogeneous (top) and a metaconcrete (bottom) slab. The typical shock wave observed in homogeneous materials is delayed in time and trapped within the aggregates as elastic oscillation energy in the resonant metaconcrete.

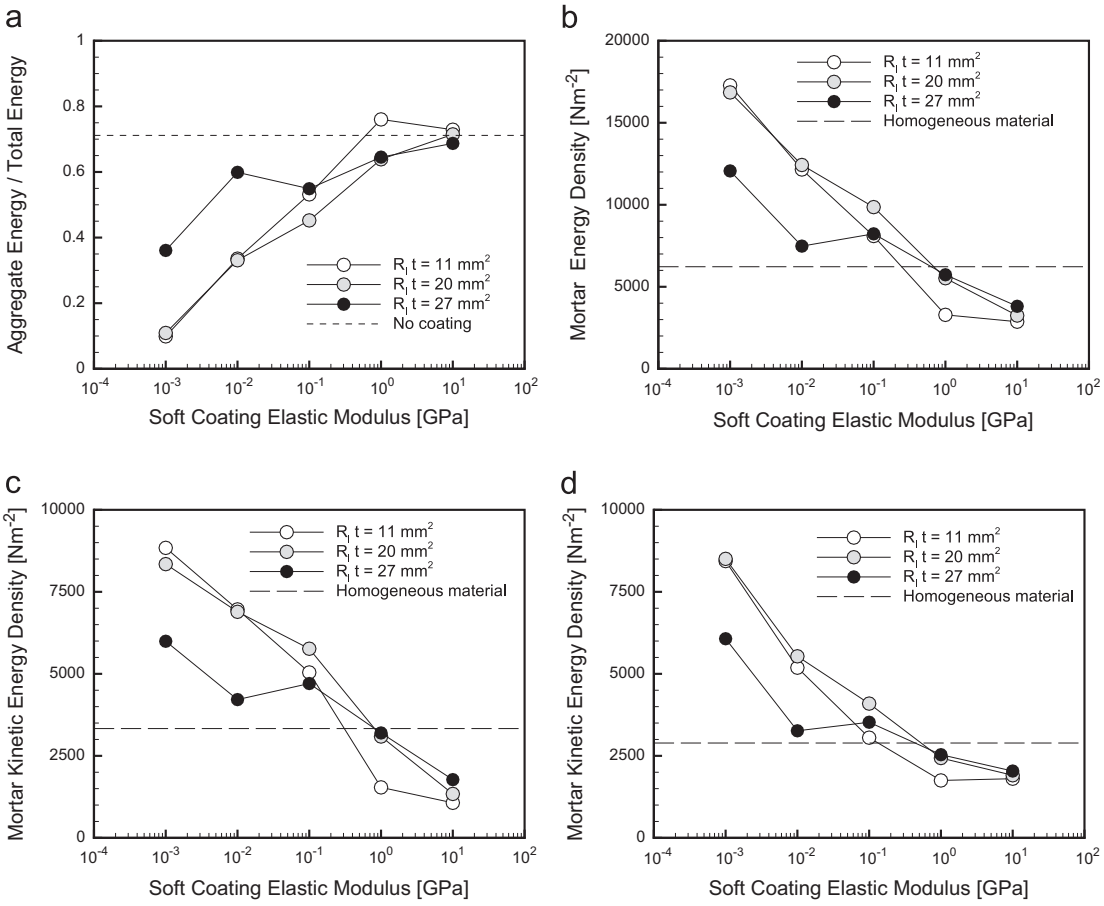

Fig. 11. Parametric study by varying the soft coating thickness and elastic modulus. (a) Fraction of the total mechanical energy captured by the aggregates; (b) average energy density of the mortar; (c) average elastic energy density of the mortar; (d) average kinetic energy density of the mortar. For each case, the results attained using an equivalent homogeneous concrete slab are also shown for comparison.

distribution of kinetic, elastic, and mechanical energies between the three phases of the metaconcrete and in terms of the maximum and minimum longitudinal stress observed in the mortar.

Fig. 11 shows the percentage of the energy captured by the aggregates as a function of the elastic modulus of the soft coating. Each line refers to a different aggregate geometry.

The plots show that, in order to transfer energy from the mortar to the heavy cores, it is necessary to have a coating softer than the other two phases but stiff enough to still transfer some stress. Very soft coatings (such as silicone, natural rubber, or polyethylene) cause the heavy core to be excluded from the dynamic behavior of the metaconcrete, and at the same time reduce the global stiffness of the system. Thus, at an equal blast force, the material deforms more and the supplied energy is higher. In these cases, the performance of the metaconcrete can be considered inferior to that of a homogeneous concrete slab, as shown by the first three points in Fig. 11(b). When the stiffness of the soft material is comparable to the stiffness of both the lead and mortar phases, the metaconcrete works as a whole and exhibits attenuation of the longitudinal stress with

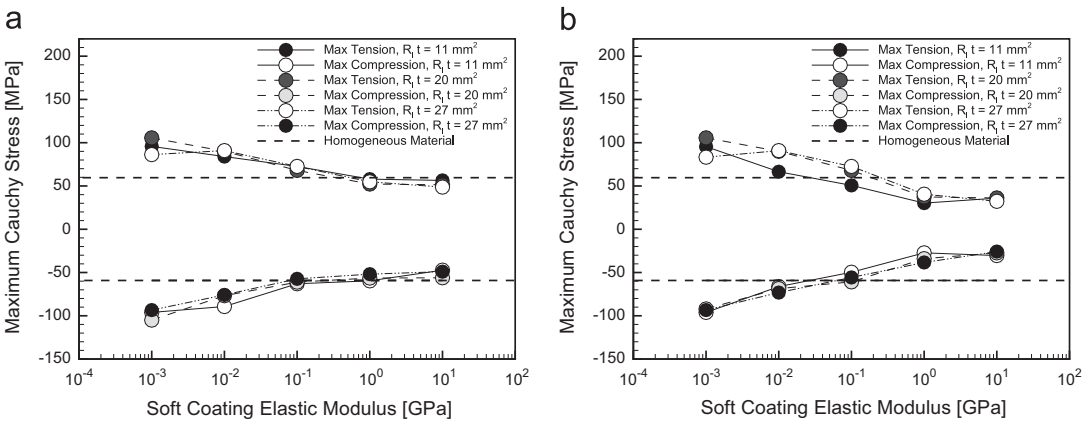

Fig. 12. Maximum and minimum longitudinal Cauchy stress in the metaconcrete slab, as a function of the soft coating elastic modulus. (a) Stresses in the full length of the slab and (b) Stresses in the half slab furthest from the blast face.

propagation of the shock wave, due to trapping of the energy within the resonant cores. The effect visualized in Fig. 10 is observed in all the configurations characterized by high modulus soft coatings, such as nylon or urea formaldehyde.

The stress cannot be reduced in the section of slab nearest to the blast exposed face. However, it is likely that the magnitude of the stress induced in the mortar reduces progressively with distance from the exposed face. Fig. 12(a) shows the maximum tensile and compressive normal stress observed in the mortar during the entire duration of the dynamical analysis. The maximum longitudinal stress in the mortar reduces with increasing soft coating stiffness. In the case of urea formaldehyde, the maximum longitudinal stress is half of the stress computed for the silicone coating.

The stress reduction is more evident when we consider only the right half of the slab, furthest from the blast site, see Fig. 12(b). In this region, the maximum stress evaluated for the urea formaldehyde coating reduces to one-fourth of the stress computed for the silicone coating. Therefore, we can ascertain that the main advantage of the bi-material aggregates described here is to reduce the amount of energy transmitted through the depth of the slab perpendicular to the blast face and, consequently, the magnitude of the stress in the mortar phase.

5. Conclusions

We have introduced a concept for a new type of concrete, where standard stone and sand aggregates are replaced by bi-material inclusions consisting of a heavy metal core coated with a softer material. These artificial aggregates may exhibit resonant behavior when excited by dynamical loading. Oscillatory behavior occurs when the natural frequencies of the internal masses are activated, and as a result the inclusions are able to adsorb a consistent fraction of the mechanical energy, reducing the total energy and the stress level in the mortar matrix. Ideally, such a material should be able to filter mechanical waves within the range of the natural frequency of the resonant aggregates. The idea exploited here has been suggested by the theoretical studies of Milton and Willis (2007), who introduced the concept of an effective mass or p-mass. The p-mass depends on the natural resonant frequencies of the system, and when the microstructure is excited near these frequencies the system can exhibit negative effective mass.

In the present study we have undertaken a numerical analysis to determine the response of an ideal system made of uniform and regularly arranged aggregates. The inclusions are spherical and their arrangement was chosen in order to produce a packed configuration of aggregates with very little separation. The numerical results show that, under dynamic excitation, the metaconcrete behaves in a rather different way to an equivalent homogeneous slab with the effective properties of concrete. The most prominent effect is the reduction in the amount of energy transmitted across the system and, as a result, the reduction of stress within the brittle phase, i.e., the mortar.

In the numerical calculations, we have considered three heavy core radii and three coating thicknesses. However, in the results obtained, we do not observe a strong dependence of the mechanical response on these geometrical parameters. Our results show that the most important parameter is the elastic modulus of the soft coating. This outer layer to the heavy core must be more compliant, although of comparable stiffness, to the mortar and lead components. Only under these conditions is the soft coating able to transfer the mechanical energy contained in the mortar to the heavy cores and, as a result, activate elastic oscillations inside the resonant aggregates. The presence of resonant aggregates attenuates the tensile and compressive stresses in the brittle mortar phase, which is most susceptible to weakening and fracture under high stresses.

The present study defines a new form of concrete capable of reducing the energy transmitted by dynamical loading without the use of dissipative elements. The analyses performed here consider only purely elastic materials and do not account for other characteristics typical of mortar, such as viscosity or brittleness. These characteristics are, however, important aspects to consider for actual applications, since exposed mortar under the action of blast loading will display extensive damage. It is also relevant to note that a portion of the supplied energy will be dissipated when fracture surfaces

are created during damage of the material, and the proportion of mechanical energy transmitted to the extended slab will be smaller than that transmitted in the purely elastic case. The stresses in this case will also be expected to reduce accordingly. Preliminary calculations accounting for fracture and damage of the mortar phase appear to confirm this behavior.

Additionally, there are practical design considerations that must be evaluated. The use of lead for the heavy core material poses a pollution issue, and may not be suitable for certain applications. Other materials with high density or metal alternatives may appropriate and will be considered in future design development. The durability, compressive strength, and static properties of the proposed composite will also be considered in an effort to develop metaconcrete as a viable concrete alternative for dynamic loading applications, while still maintaining the integrity of regular concrete as used for construction purposes.

The careful consideration and assessment of the effect of viscosity and brittleness, the experimental validation of theoretical models and designs, and further improvements to the basic designs explored in the present work suggest themselves as worthwhile avenues for future research.

Acknowledgments

This research was supported by the Air Force of Scientific Research Grant # FA9550-12-1-0091 through the University Center of Excellence in High-Rate Deformation physics of Heterogeneous Materials and is gratefully acknowledged.

Appendix A

The blast is modeled as follows. An explosion in air of pressure p_0 produces an overpressure, $p(t)$, in the surrounding atmosphere. This is called the blast wave. At a fixed, reasonable distance r from the center of the explosion, all overpressure histories due to any blast are similar, see Fig. 13. In particular, the shock velocities are uniquely related to the overpressure ratios, thus the peak overpressure uniquely defines the time required for the shock front to travel out to various distances and the decay time to reach the original pressure p_0. It follows that the shock pressure front reaches the position r at time $t = t_r$. Thus, the air pressure at the observer location jumps to the initial overpressure $p_0 + P$. The overpressure immediately begins to decay, following a pressure–time relation described by the following quasi-exponential relation (A.1), known as the modified Friedlander equation:

$$p(t) = p_0 + P(1-\tau)\exp(-b\tau), \quad \tau = \frac{t-t_r}{T_d}, \quad t > t_r \tag{A.1}$$

where T_d is the duration of the positive overpressure phase and b is a decay parameter.

The characteristics of blast waves caused by explosions have been obtained using both experimental and analytical means. Values for the parameters of a blast shock wave generated in a nominal standard atmosphere by a 1 ton spherical charge of *TNT*[1] are tabulated in Kinney (1962). Applying a simple scaling principle, two explosions in atmosphere can be expected to give identical blast wave intensities at distances which are proportional to the cube root of the respective energy release. The controlling item for explosions in atmosphere is yield factor λ, i.e., the energy release W per unit quantity of the surrounding medium divided by the energy of the reference explosion in air, i.e.,

$$\lambda = \left(\frac{W}{W_{\text{ref}}}\right)^{1/3}. \tag{A.2}$$

The operative procedure to compute the scaled parameters can be found elsewhere (Kinney, 1962), and these computations have been implemented in the finite element code used in the present calculations.

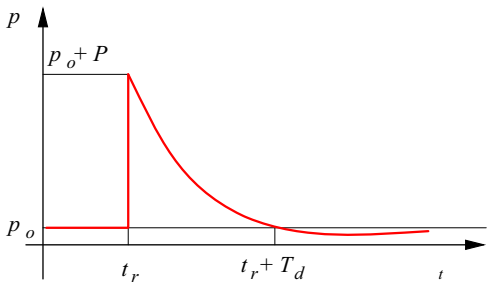

Fig. 13. Typical pressure–time curves for an explosive blast wave.

References

Brun, M., Guenneau, S., Movchan, A.B., 2009. Achieving control of in-plane elastic waves. Appl. Phys. Lett. 94. 061903/1–3.
Gibiansky, L.V., Sigmund, O., 2000. Multiphase composites with extremal bulk modulus. J. Mech. Phys. Solids 48, 461–498.
Goffaux, C., Sánchez-Dehesa, J., 2003. Two-dimensional phononic crystals studied using a variational method: application to lattices of locally resonant materials. Phys. Rev. B 67 (14), 144301.
Hirsekorn, M., 2004. Small-size sonic crystals with strong attenuation bands in the audible frequency range. Appl. Phys. Lett. 84 (17), 3364–3366.
Jensen, J.S., 2003. Phononic band gaps and vibrations in one- and two-dimensional mass-spring structures. J. Sound Vib. 266 (5), 1053–1078.
Kinney, G.F., 1962. Explosive Shocks in Air. The MacMillan Company, New York.
Klironomos, A.D., Economou, E.N., 1998. Elastic wave band gaps and single scattering. Solid State Commun. 105 (5), 327–332.
Kundtz, N., Smith, D.R., 2010. Extreme-angle broadband metamaterial lens. Nat. Mater. 9 (2), 129–132.
Kushwaha, M.S., Halevi, P., Dobrzynski, L., Djafari-Rouhani, B., 1993. Acoustic band structure of periodic elastic composites. Phys. Rev. Lett. 71 (13), 2022–2025.
Liu, Z., Zhang, X.X., Mao, Y., Zhu, Y.Y., Yang, C.T., Chan, Z., Sheng, P., 2000. Locally resonant sonic materials. Science 289, 1734–1736.
Liu, Z., Chan, C.T., Sheng, P., 2002. Three-component elastic wave band-gap material. Phys. Rev. B 65 (165116), 1–6.
Liu, Z., Chan, C.T., Sheng, P., 2005. Analytic model of photonic crystals with local resonances. Phys. Rev. B 71. 014103/1–8.
Liu, Z., Hu, G.K., Huang, G.L., Sun, C.T., 2011. An elastic metamaterial with simultaneously negative mass density and bulk modulus. Appl. Phys. Lett. 98. 251907/1–3.
Liu, A.P., Zhu, R., Liu, X.N., Hu, G.K., Huang, G.L., 2012. Multi-displacement microstructure continuum modeling of anisotropic elastic metamaterials. Wave Motion 49 (3), 411–426.
Mei, J., Liu, Z., Wen, W., Sheng, P., 2006. Effective mass density of fluid-solid composites. Phys. Rev. Lett. 96 (2), 024301.
Milton, G.W., 2007. New metamaterials with macroscopic behavior outside that of continuum elastodynamics. New J. Phys. 9 (10), 359.
Milton, G.W., Willis, J.R., 2007. On modifications of Newton's second law and linear continuum elastodynamics. Proc. R. Soc. A 463, 855–880.
Milton, G.W., Briane, M., Willis, J.R., 2006. On cloaking for elasticity and physical equations with a transformation invariant form. New J. Phys. 8 (10), 248.
Pendry, J.B., 2000. Negative refraction makes a perfect lens. Phys. Rev. Lett. 85 (18), 3966–3969.
Psarobas, I.E., Stefanou, N., Modinos, A., 2000. Scattering of elastic waves by periodic arrays of spherical bodies. Phys. Rev. B 62 (1), 278–291.
Sheng, P., Zhang, X.X., Liu, Z., Chan, C.T., 2003. Locally resonant sonic materials. Physica B 338, 201–205.
Sheng, P., Mei, J., Liu, Z., Wen, W., 2007. Dynamic mass density and acoustic metamaterials. Physica B: Condens. Matter 394 (2), 256–261.
Sigmund, O., 2000. A new class of extremal composites. J. Mech. Phys. Solids 48, 397–428.
Sigmund, O., Torquato, S., 1997. Design of materials with extreme thermal expansion using a three-phase topology optimization method. J. Mech. Phys. Solids 45 (6), 1037–1067.
Wang, G., Wen, J., Liu, Y., Wen, X., 2004a. Lumped-mass method for the study of band structure in two-dimensional phononic crystals. Phys. Rev. B 69 (18), 184302.
Wang, G., Wen, X., Wen, J., Shao, L., Liu, Y., 2004b. Two-dimensional locally resonant phononic crystals with binary structures. Phys. Rev. Lett. 93 (15), 154302.
Wang, G., Yu, D., Wen, J., Liu, Y., Wen, X., 2004c. One-dimensional phononic crystals with locally resonant structures. Phys. Lett. A 327 (5–6), 512–521.
Wang, G., Wen, X., Wen, J., Liu, Y., 2006. Quasi-one-dimensional periodic structure with locally resonant band gaps. J. Appl. Mech. 73 (1), 167–170.
Xiao, Y., Wen, J., Wen, X., 2012. Longitudinal wave band gaps in metamaterial-based elastic rods containing multi-degree-of-freedom resonators. New J. Phys. 14 (3), 033042.
Zhu, R., Huang, H.H., Huang, G.L., Sun, C.T., 2011. Microstructure continuum modeling of an elastic metamaterial. Int. J. Eng. Sci. 49 (12), 1477–1485.

[1] A gram of TNT releases 4200–4602 J upon explosion. This was arbitrarily standardized by setting 1 g of TNT=4184 J and called the tonne of TNT.